Pacific Northwest
NATIONAL LABORATORY

PNNL-38532

Atomistic Modeling of the Interphase Structure between Alumina and Al12Fe2Cr Quasicrystal Approximant

September 2025

Wahyu Setyawan
Krishna C Pitike

U.S. DEPARTMENT of ENERGY

Prepared for the U.S. Department of Energy
under Contract DE-AC05-76RL01830

DISCLAIMER

PACIFIC NORTHWEST NATIONAL LABORATORY
operated by
BATTELLE
for the
UNITED STATES DEPARTMENT OF ENERGY
under Contract DE-AC05-76RL01830

Printed in the United States of America

Available to DOE and DOE contractors from
the Office of Scientific and Technical Information,
P.O. Box 62, Oak Ridge, TN 37831-0062
www.osti.gov
ph: (865) 576-8401
fox: (865) 576-5728
email: reports@osti.gov

Available to the public from the National Technical Information Service
5301 Shawnee Rd., Alexandria, VA 22312
ph: (800) 553-NTIS (6847)
or (703) 605-6000
email: info@ntis.gov
Online ordering: http://www.ntis.gov

PNNL-38532

Atomistic Modeling of the Interphase Structure between Alumina and Al12Fe2Cr Quasicrystal Approximant

September 2025

Wahyu Setyawan
Krishna C Pitike

Prepared for
the U.S. Department of Energy
under Contract DE-AC05-76RL01830

Pacific Northwest National Laboratory
Richland, Washington 99354

Summary

Molecular dynamics simulations are performed to study the stability of an fcc metallic interlayer phase between an iron aluminide quasicrystal approximant (QCA) phase (84.2 Al, 5.7 Fe, 5.4 Ni, and 4.7 at.% Cr) and aluminum oxides (α-Al_2O_3 and γ-Al_2O_3). The presence of the interlayer phase was experimentally observed in some regions of the inner diameter surface of a TPBAR cladding tube. The simulations employed existing many-body (MEAM and EAM) interatomic potentials to describe atomic interactions in the interlayer and QCA phases, and Buckingham+Coulomb pair interactions for the alumina and between the alumina and the QCA (or fcc). Interface systems of QCA/alumina, fcc/alumina, and QCA/fcc are modeled and the fracture energy of the interfaces is calculated. Based on the fracture energies, for the γ-Al_2O_3, both MEAM and EAM suggest that the fcc interlayer phase would not form. For the α-Al_2O_3, the MEAM predicts that the fcc phase would form, however, the EAM predicts that it forms only if the α-Al_2O_3 is Al-terminated at the interface. For the O-terminated α-Al_2O_3, the EAM predicts the fcc phase would not form, consistent with the results for γ-Al_2O_3.

Acknowledgments

This research was supported by the National Nuclear Security Administration (NNSA) of the U.S. Department of Energy (DOE) through the Tritium Science Research Supporting the Tritium Modernization Program (TMP) managed by Pacific Northwest National Laboratory (PNNL). A portion of the calculations is performed using PNNL Research Computing.

1.0 Introduction

Recent post-irradiation characterization of cycle 13 iron aluminide coated 316SS cladding revealed complex microstructures [1]. In general, when iron aluminide coating is applied to 316SS, it forms an interface region, a columnar region (the middle region), and a functional region (the outer region). Each region consists of complex phases. This project focuses on the outer region where the main phase exhibits a diffraction pattern resembling that of a quasicrystal approximant phase (QCA) $Al_{12}Fe_2Cr$ [2], although there are discrepancies where not all spot intensities are correct. The discrepancies are presumably caused by composition differences where the characterization shows a composition of 78.9 Al, 9.3 Fe, 6.0 Cr, and 5.7 at.% Ni, rather than stoichiometric $Al_{12}Fe_2Cr$. Due to oxidation of the iron aluminide coating, two alumina phases were observed on the surface of the QCA. The first oxide was identified as corundum (α-Al_2O_3), which forms a dense film with a relatively uniform thickness (~20 nm). The other oxide was identified as polycrystalline γ-Al_2O_3, which forms a porous film with non-uniform thicknesses (can reach several μm). STEM(ADF) tilt series showed pores ranging from 10 to 100 nm were observed throughout the γ-Al_2O_3. It is currently unknown why some surface regions of the QCA oxidized into α-Al_2O_3, while other surface regions oxidized into γ-Al_2O_3.

Further characterization [3] revealed that the interface between the oxides and the QCA exhibits a transition layer with a crystal structure that is different from the underlying base QCA structure. The transition layer (interphase structure) appears to be an fcc or a close-packed metallic layer on the order of 1-2 nm thick. Compared to the composition of the QCA, the interphase structure exhibits depletion of Al, but enrichment of Fe and Cr. The goal of this project is to determine the interface structures of oxide/interphase-structure/QCA (oxide/IPS/QCA) by employing atomistic modeling. We will employ classical interatomic potentials and a hybrid molecular dynamic / Monte Carlo (MD/MC) simulation technique to evolve the structure of the transition layer. Slab systems of oxide/IPS/QCA will be constructed with an fcc IPS. A transition region will be defined to include the IPS and a portion of oxide and QCA close to the IPS. Hybrid MD/MC simulations will be performed to evolve the system towards thermodynamically preferred configuration. The hybrid technique allows for faster evolution of the system by incorporating MC swaps of metal atoms within the transition region. Metropolis algorithm will be used for the acceptance or rejection probability of the swap, based on the energy change. Different slab orientations will be studied.

2.0 Method

2.1 Density Functional Theory

Density functional theory (DFT) calculations are performed to test existing interatomic potentials (IAPs). The test is done to compare the stability of QCA versus fcc solid solution. Section 2.2. describes the IAPs to be tested. The DFT calculations are performed using the VASP software, employing the latest PAW-PBE64 pseudopotentials. The valence electrons for Fe, Ni, Cr, and Al are 8, 10, 6, and 3, respectively. The energy cutoff for expanding the planewaves is 350 eV. The Brillouin zone is sampled with Γ-centered KPOINT grid of 3x3x1. The self-consistent field (SCF) loop is converged within 10^{-5} eV. Structures are relaxed with a force convergence of 0.025 eV/Å, allowing both simulation cell and atomic positions to relax.

2.2 Interatomic Potentials

To describe Al, Cr, Fe, and Ni interactions in the QCA and fcc interlayer, two many-body IAPs are tested. The first one is an embedded-atom method (EAM) potential [4], developed in 2020 to study fcc high-entropy alloys. The second one is a modified-embedded-atom method (MEAM) potential [5], developed in 2025 to study bcc and fcc multi-principal-element alloys. The potentials are tested for their ability to predict the stability order between QCA and fcc structures. Since diffraction patterns resembling those of a QCA were observed experimentally in the inner surface region of the iron aluminide coated 316SS tube, the QCA is expectedly more stable than fcc at the composition observed in the experiment, namely approximately 81.52 Al, 6.5 Fe, 6.32 Ni, and 5.66 at.% Cr, deduced from an EDS line scan from [3], reproduced in Fig. 1.

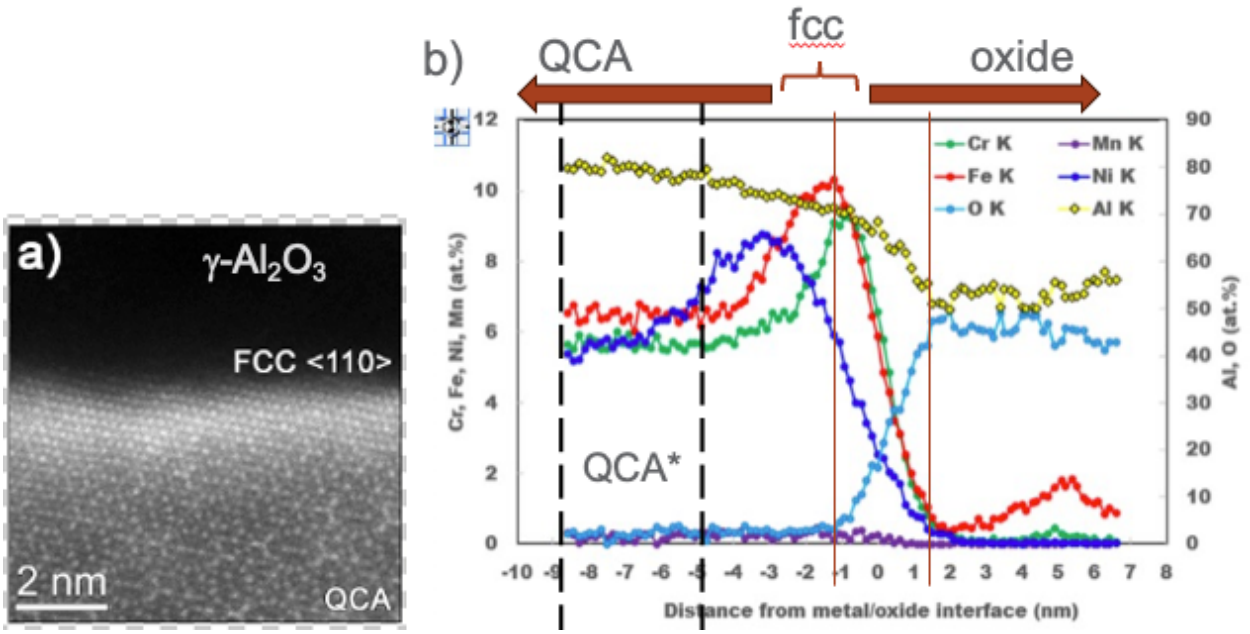

Figure 1. a) STEM-HAADF image of a surface region of the inner diameter (ID) surface of a TPBAR cladding tube, b) EDS line scan across interfaces, where the region denoted as QCA* is the composition from which a QCA model is constructed for simulations.

To construct a QCA model, the $Al_{12}Fe_2Cr$ QCA structure from [2] is adopted as a prototype. This prototype has 266 Al sites and 50 transition metal (TM) sites, where each TM site is a mixture of 67% Fe and 33% Cr. Using an Fe-Cr-Al machine learning potential developed under the performance modeling activity, Fe and Cr preferred sites are determined among the 50 TM sites. The result shows there are 26 Fe preferred sites, 16 Cr preferred sites, and 8 random Fe or Cr sites, as shown in Figure 1. To construct the QCA model, the 8 random Fe/Cr sites are assigned as Ni. In addition, randomly selected 8 out of 26 Fe preferred sites and 1 out of 16 Cr preferred sites are assigned as Ni. Thus, the final composition of the QCA model, denoted as QCA*, is 266 Al (84.2%), 18 Fe (5.7%), 17 Ni (5.4%), and 15 Cr (4.7%). For the test, 50 QCA* configurations and 50 configurations of random fcc solid solution are constructed. The fcc structures are constructed using a supercell containing 256 atoms with a composition 215 Al (84.0%), 15 Fe (5.8%), 14 Ni (5.5%), and 12 Cr (4.7%). Subsequently, the energies of these configurations are calculated with EAM, MEAM, and DFT. All molecular dynamics simulations are performed with the LAMMPS software. DFT predicts that QCA is more stable than fcc by 40 meV/atom. MEAM agrees with DFT, but the QCA is only 4 meV/atom more stable than fcc. On the contrary, EAM predicts fcc is more stable than QCA by 135 meV/atom.

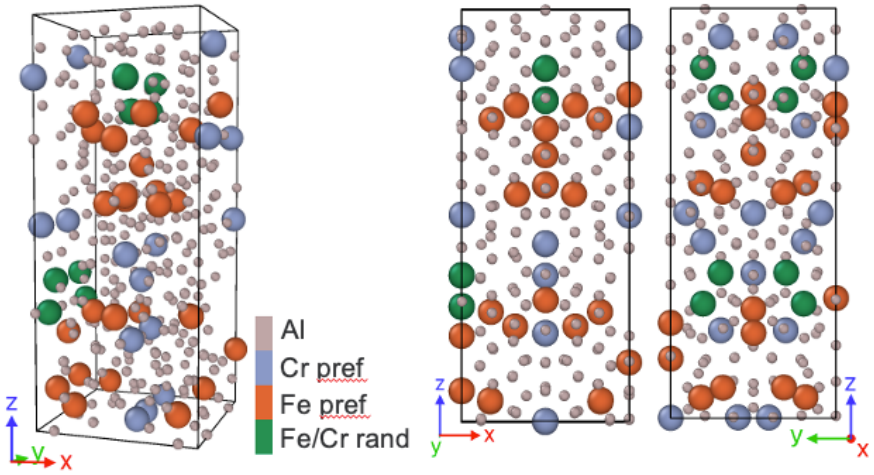

Figure 2. Structure of $Al_{12}Fe_2Cr$ QCA structure where the Cr preferred sites, Fe preferred sites, and Fe/Cr random sites are determined with a Fe-Cr-Al machine learning potential.

Buckingham + Coulomb potentials are employed to describe interactions in alumina and between the alumina and the QCA (or fcc):

$$E(r) = A \exp\left(\frac{-r}{\rho}\right) - \frac{C}{r^6} + \text{Coulomb}$$

The parameters of the Buckingham interactions are given in Table 1. The Buckingham interactions for metal-metal atoms are zero. The Coulomb interactions to be used with the Buckingham interactions are calculated with the elemental charges of -2 (O), +3 (Al, Fe, and Cr), and +2 (Ni).

Table 1. Parameters for the Buckingham interactions.

	A (eV)	ρ (Å)	C (eVÅ^6)	ref
O-O	9547.96	0.2192	32	[6]
Al-O	1725.2	0.28971	0	[6]
Cr-O	1204.18	0.3165	0	[7]
Fe-O	1414.6	0.3128	0	[8]
Ni-O	905.4	0.3145	0	[9]

The Buckingham+Coulomb potential cannot be used together with the MEAM potential because the Coulomb potential requires atomic charges while the metal atoms in the QCA and the interlayer, that are modeled with the MEAM potential, do not have charges. Therefore, the Buckingham+Coulomb potentials are converted into a table style so that atomic charges will no longer be needed during simulations. A Coulomb interaction is a long-range interaction, i.e. no cutoff distance, which is typically evaluated in the reciprocal space with a Fourier transform. On the other hand, a potential table requires a cutoff distance. To determine the appropriate cutoff distance, various sets of potential tables for Al-Al, Al-O, and O-O are generated with various cutoff distances and tested against their ability to produce stable alumina structures. To generate a potential table, the Buckingham+Coulomb interaction is evaluated as a long-range interaction using *bouk/coul/long pair_style* within LAMMPS using a 15x15x15 supercell of the α-Al_2O_3, then the pair energies and forces are evaluated as a function of distance and written out to a potential table file. Figure 3 shows snapshots of α-Al_2O_3 structure at 300 K simulated with several cutoff distances. At cutoff of 4.6 Å or shorter, the crystalline structure is unstable and becomes amorphous. A stable crystal is obtained with a cutoff of 4.77 Å. By analyzing the atom pair distribution function shown in Figure 4, it is revealed that there is an Al-O peak at 4.675 Å which needs to be included to produce a stable crystal. On the other hand, there are Al-Al and O-O peaks at 4.815 Å which needs to be excluded. Therefore, a cutoff of 4.77 Å is selected. Further tests in γ-Al_2O_3 also confirm that this cutoff is appropriate.

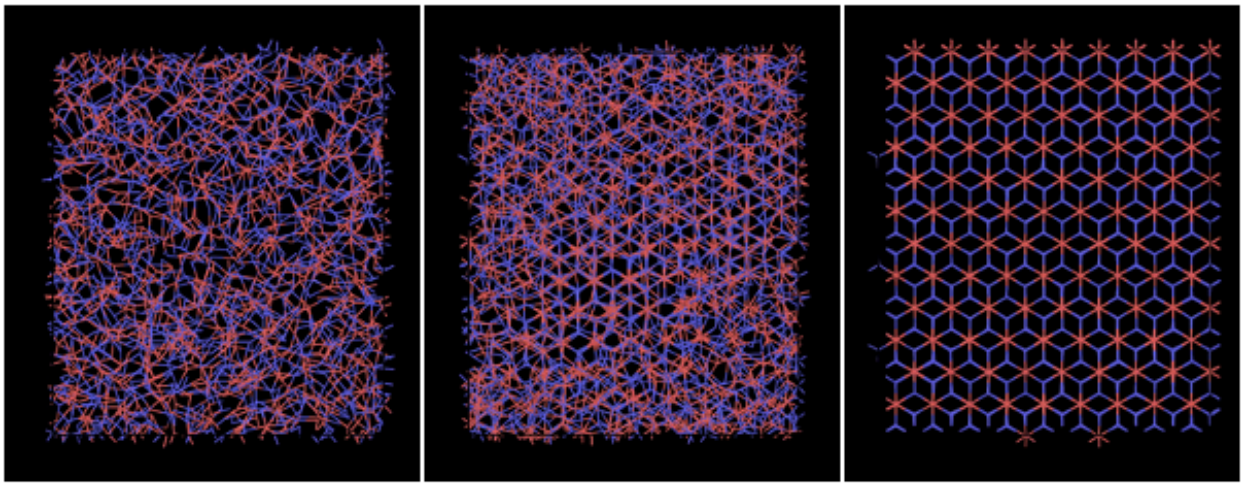

Figure 3. Snapshots of α-Al_2O_3 structure at 300 K simulated with Buckingham+Coulomb potential tables with a cutoff of 4.1, 4.6, and 4.77 Å which

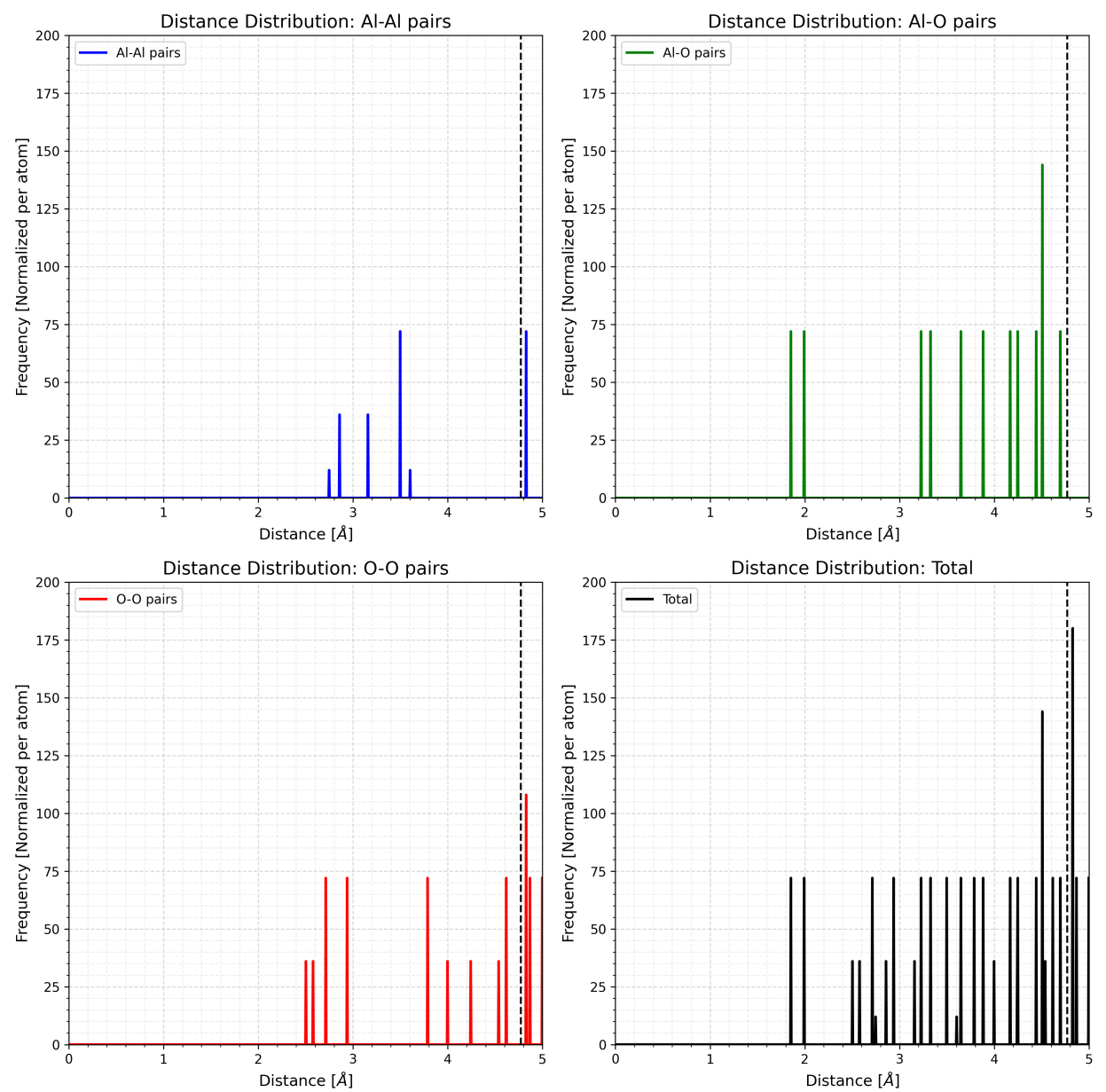

Figure 4. Pair distribution function of α-Al_2O_3 at zero K. The vertical dashed line denotes the cutoff distance of potential tables of the Buckingham+Coulomb interactions at 4.77 Å that produces stable alumina crystals.

2.3 Interfaces Studied

Initially we plan to perform MD/MC (molecular dynamic/monte carlo) simulations to evolve the interlayer metal to see if it will transform into a QCA or remains fcc to study its stability. Unfortunately, the MEAM potential, which correctly predicts QCA to be more stable than fcc, incorrectly predicts that an amorphous structure is more stable than fcc. Therefore, the MD/MC simulations with the MEAM potential will evolve the interlayer structure towards amorphous. Thus, MD/MC simulations cannot be performed. As an alternative to study the stability of the fcc

interlayer, we construct interfaces of QCA/alumina, alumina/fcc, and QCA/fcc and calculate the fracture energies. For the QCA, α-Al_2O_3, and γ-Al_2O_3, slabs with (001) surface are studied. For the fcc, slabs with (001), (110), and (111) surfaces are studied. For the QCA/alumina and QCA/fcc interfaces, the QCA are taken as the substrate. For the alumina/fcc interfaces, the alumina is assumed as the substrate because the oxide is much thicker than the interlayer, as indicated in experiments. An interface system is constructed by assuming that the substrate is unstrained in the lateral dimensions. Subsequently, supercells of the substrate and the top slab that minimize the strain to the top slab are determined and used to construct the interface system. Table 2 lists 11 interfaces that are studied, including the lattice parameters of each crystal and the supercells of the top slabs and substrates used to construct the interfaces. Table 3 shows the lattice strain of the top slabs. To get statistics, for each interface system, nine models are generated by laterally shift (x and y) the top slab with respect to the substrate using a 3x3 grid of the unit cell of the substrate.

Table 2. Lattice parameters, a and b, along the first and second lattice vectors of the lateral dimension of the top slabs and substrates, respectively, and the corresponding supercells, Na and Nb used to construct 11 interface systems.

	Slab (top slab)						
interface index	slab	a	b	Na	Nb	Na*a	Nb*b
1	α−Al2O3	8.33	4.81	6	8	49.96	38.46
2	γ−Al2O3	7.95	7.95	11	13	87.41	103.31
3	FCC-001	2.80	2.80	15	24	41.95	67.12
4	FCC-110	3.96	2.80	21	24	83.06	67.12
5	FCC-111	4.84	2.80	12	24	58.13	67.12
6	FCC-001	2.80	2.80	17	17	47.54	47.54
7	FCC-110	3.96	2.80	20	17	79.10	47.54
8	FCC-111	4.84	2.80	18	17	87.19	47.54
9	FCC-001	2.80	2.80	27	23	75.51	64.32
10	FCC-110	3.96	2.80	16	23	63.28	64.32
11	FCC-111	4.84	2.80	13	23	62.97	64.32
	Substrate						
	substrate	a	b	Na	Nb	Na*a	Nb*b
1	QCA	12.57	12.88	4	3	50.27	38.63
2	QCA	12.57	12.88	7	8	87.97	103.02
3	α−Al2O3	8.33	4.81	5	14	41.63	67.30
4	α−Al2O3	8.33	4.81	10	14	83.26	67.30
5	α−Al2O3	8.33	4.81	7	14	58.28	67.30
6	γ−Al2O3	7.95	7.95	6	6	47.68	47.68
7	γ−Al2O3	7.95	7.95	10	6	79.47	47.68
8	γ−Al2O3	7.95	7.95	11	6	87.41	47.68
9	QCA	12.57	12.88	6	5	75.40	64.39
10	QCA	12.57	12.88	5	5	62.84	64.39
11	QCA	12.57	12.88	5	5	62.84	64.39

Table 3. Lattice strain of the top slabs in the interface systems to match the supercell of the substrates.

interface index	slab	substrate	δa [Å]	δb [Å]	δa [%]	δb [%]
1	α−Al2O3	QCA	0.31	0.18	0.62	0.44
2	γ−Al2O3	QCA	0.55	-0.28	0.64	-0.28
3	FCC-001	α−Al2O3	-0.32	0.18	-0.76	0.27
4	FCC-110	α−Al2O3	0.20	0.18	0.24	0.27
5	FCC-111	α−Al2O3	0.15	0.18	0.26	0.27
6	FCC-001	γ−Al2O3	0.14	0.14	0.29	0.29
7	FCC-110	γ−Al2O3	0.37	0.14	0.47	0.29
8	FCC-111	γ−Al2O3	0.22	0.14	0.25	0.29
9	FCC-001	QCA	-0.11	0.07	-0.15	0.11
10	FCC-110	QCA	-0.45	0.07	-0.70	0.11
11	FCC-111	QCA	-0.14	0.07	-0.21	0.11

Figure 5 shows the crystal structure of the alumina. For the α-Al_2O_3, the layering along the c-axis shows Al layer, O layer, and so on. Exposing the Al layer to the interface is denoted as Al-terminated interface. For the γ-Al_2O_3, the layering is Al layer, Al+O layer, and so on. The Al sites in the γ-Al_2O_3 have a partial occupancy of 0.889. For the interface system, after the supercell of the γ-Al_2O_3 is determined for each interface system, Al atoms are randomly deleted to model the partial occupancy.

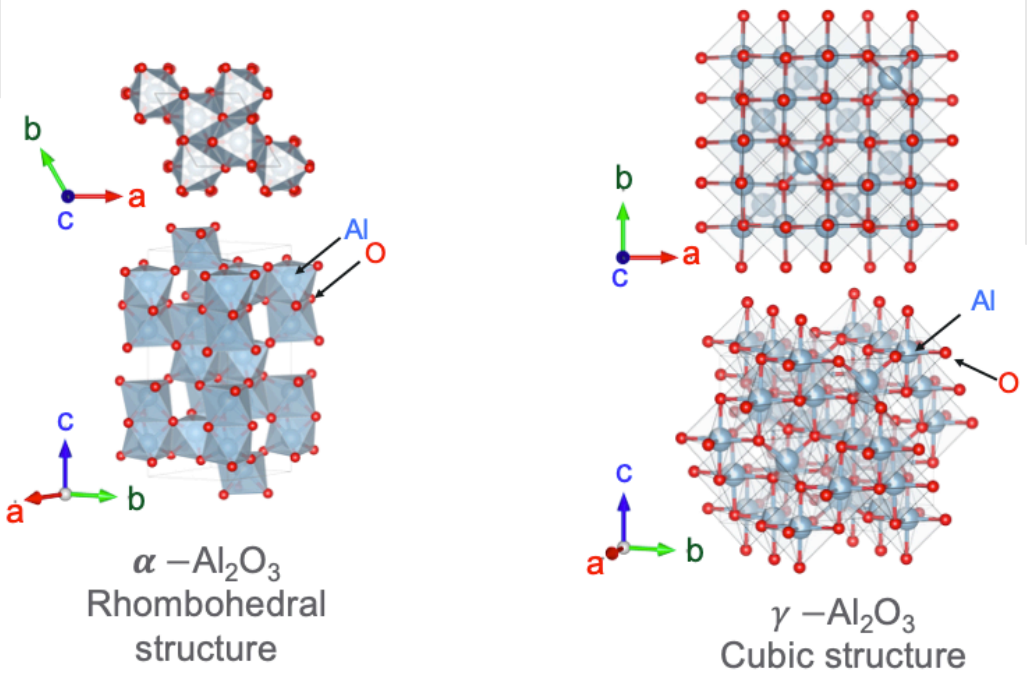

Figure 5. Structure of alumina. For the γ alumina, the Al sites have a partial occupancy of 0.889.

The following procedure is employed to construct the interface structure. Before the interface structure is constructed, each slab of the interface structure (top slab and substrate) is relaxed separately. The relaxation is done with MD relaxation at near zero K (1 K), followed by static energy minimization. Applying a static minimization directly from a configuration that is far from optimized may cause excessive atom displacements that are unrealistic. On the other hand, MD relaxation can be done more smoothly because the timestep can be adjusted. An adaptive timestep is employed for all relaxations in this study corresponding to a maximum atomic displacement of 0.01 Å per timestep or 1 fs, whichever is smaller.

Both slabs are then brought near each other with an initial separation distance of z_{sep} = 1 Å. In stage 1, the alumina slab is frozen, while the metal slab is allowed to move as a rigid body so that move along x y (in addition to z) automatically to find a preferred lateral position. MD relaxation as described above is employed. In stage 2, the metal slab is allowed to relax fully (no longer constrained as a rigid body) with MD relaxation in stage 3, energy minimization is performed for final interface structure optimization.

For the α-Al_2O_3, in stage 1 the slabs repel each other, regardless of the Al termination or O termination. Therefore, stage 1 is not performed. Different values of z_{sep} are simply tried, for each trial, stage 2 and 3 are performed. We found that at some z_{sep}, atom relaxation can result in an overall attraction between the slabs, where they would have repelled if the atom movement in the metal slab is constrained as a rigid body movement. The final configuration that produced the most optimized interface is then taken. For α-Al_2O_3, we study both Al and O terminated interfaces.

For the γ-Al_2O_3, the Al+O termination allows the alumina and metal slabs to naturally attract each other, thus no need for the Al-terminated alumina slab which repels the metal slabs. Therefore,

only Al+O terminated interfaces are studied for γ-Al_2O_3, and for brevity, we drop the termination notation for this alumina.

3.0 Results

3.1 Results with MEAM Potentials

Figures 6-12 show the initial and relaxed structures of QCA/γ-Al_2O_3, γ-Al_2O_3/fcc, and QCA/fcc obtained with the MEAM potentials + Buck/Coul potential tables. Figure 13 shows the initial and relaxed structures of QCA/α-Al_2O_3 interface with Al and O termination. Figure 14 shows the initial and relaxed structures of fcc(001)/α-Al_2O_3 interface with Al and O termination. The fracture energy of interfaces is summarized in Figure 15. The fracture energy is calculated as the following,

$$E_{fr} = \frac{1}{A}(E_{slab} + E_{substrate} - E_{interface})$$

where E_{slab}, $E_{substrate}$, and $E_{interface}$ denote the total energy of the top slab, the substrate slab, and the interface system. A is the surface area of the interface system, which is the same as for the top slab and substrate. The results indicate that the fcc interlayer formation is not preferred between the QCA and γ-Al_2O_3, however it is preferred between the QCA and α-Al_2O_3.

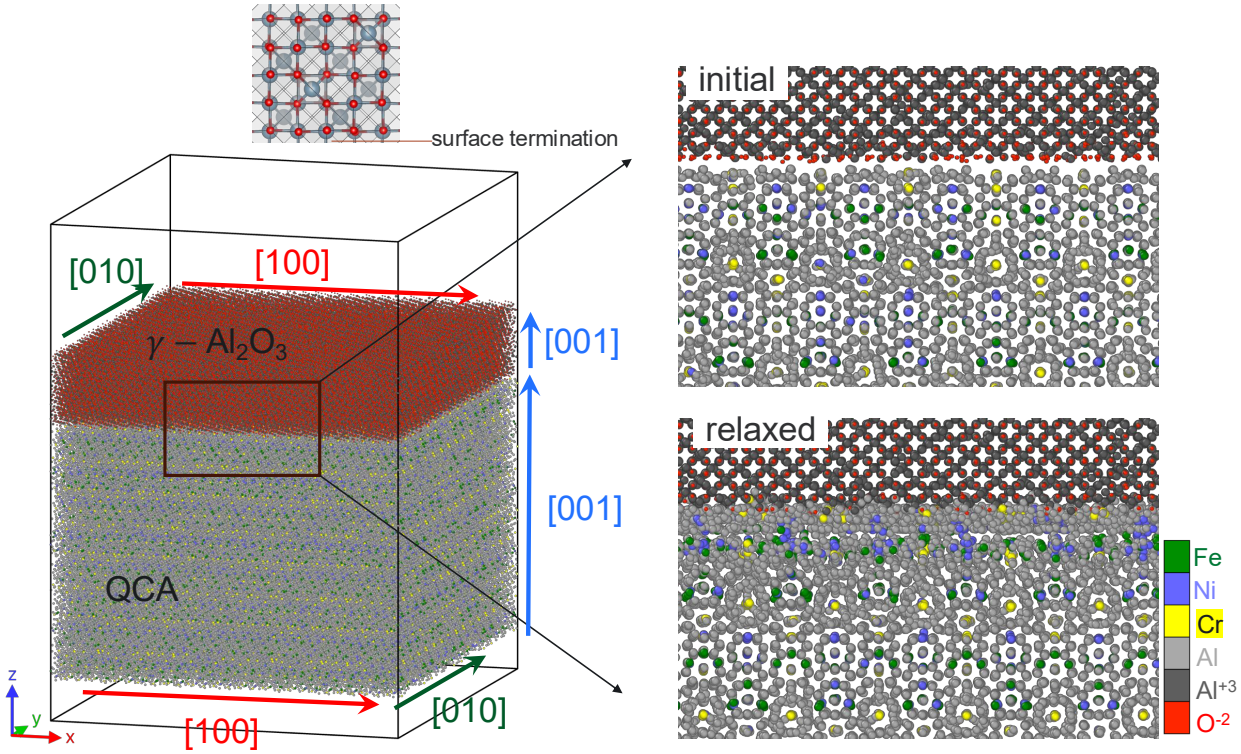

Figure 6. Crystal orientation, initial, and relaxed structures of QCA/γ-Al_2O_3 interface.

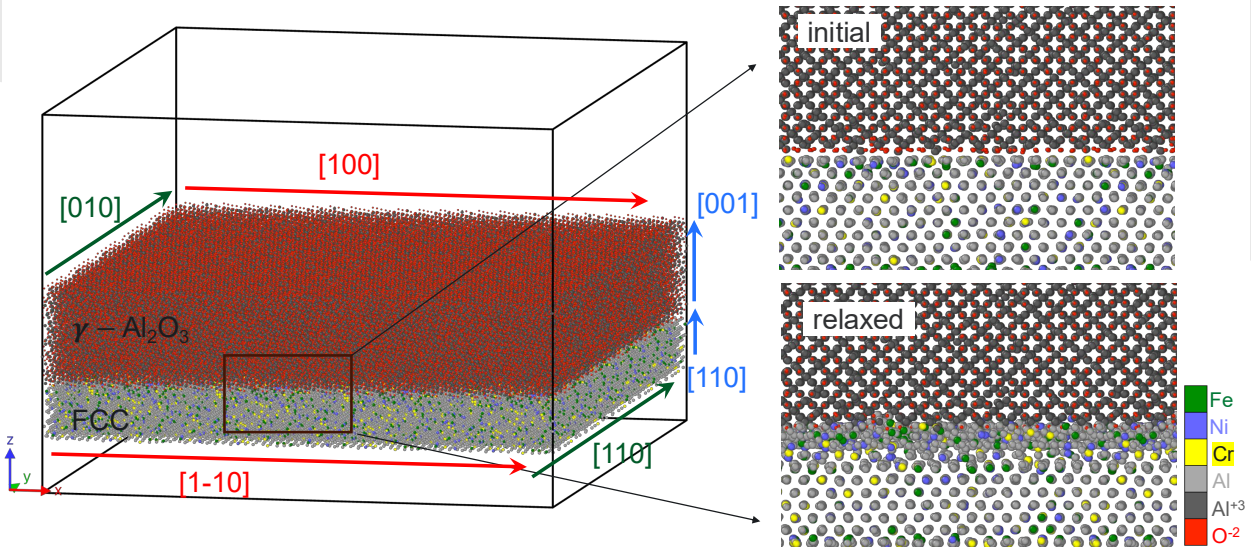

Figure 7. Crystal orientation, initial, and relaxed structures of γ-Al_2O_3/fcc(001) interface.

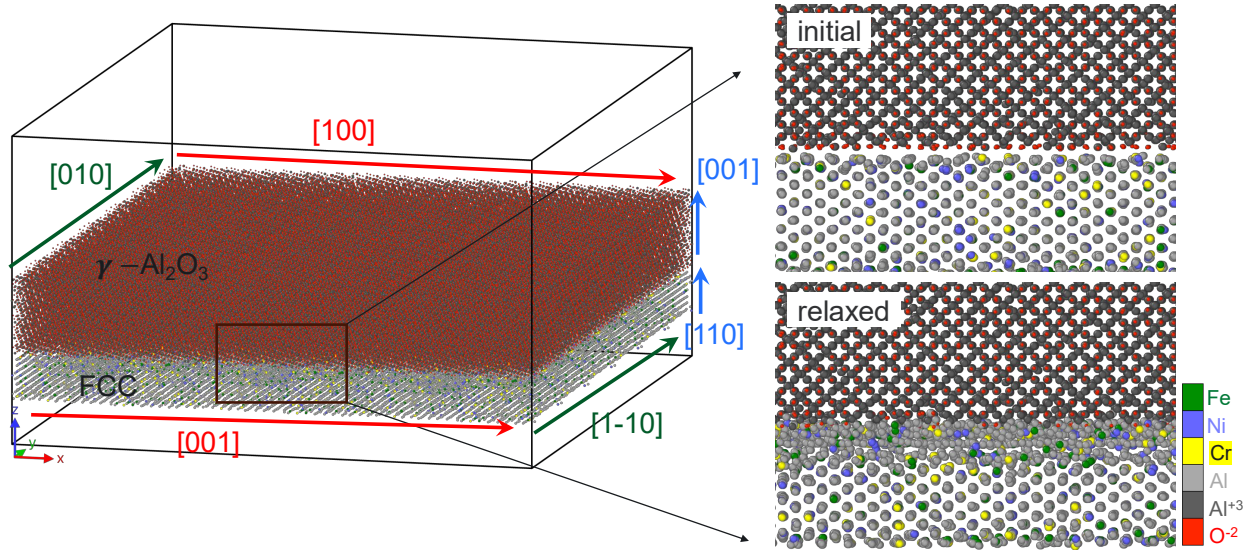

Figure 8. Crystal orientation, initial, and relaxed structures of γ-Al_2O_3/fcc(110) interface.

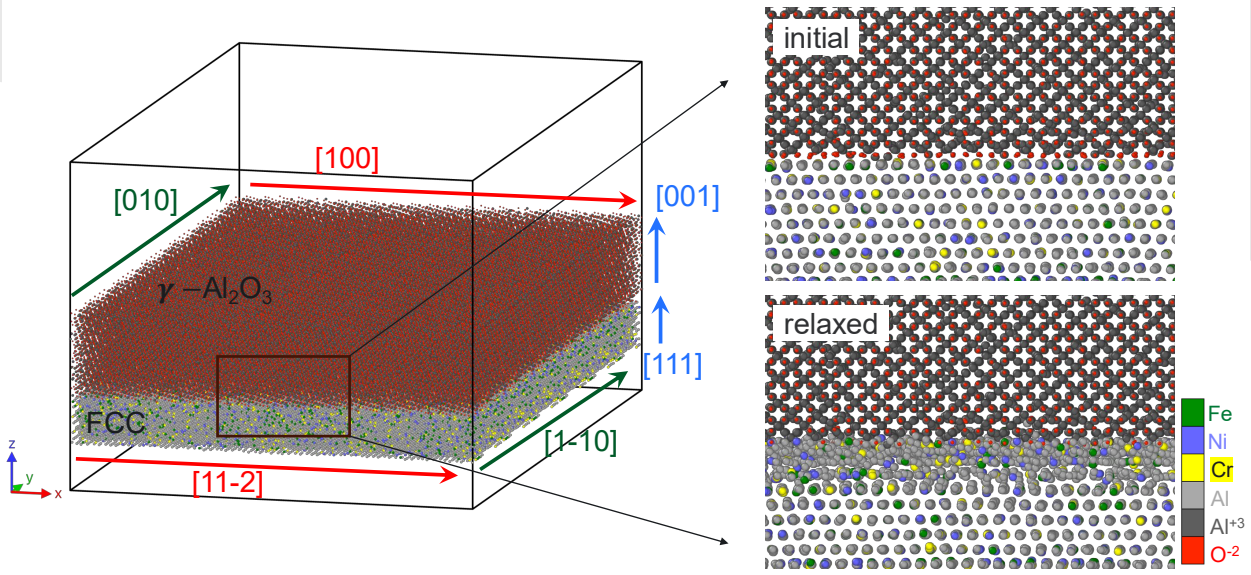

Figure 9. Crystal orientation, initial, and relaxed structures of γ-Al_2O_3/fcc(111) interface.

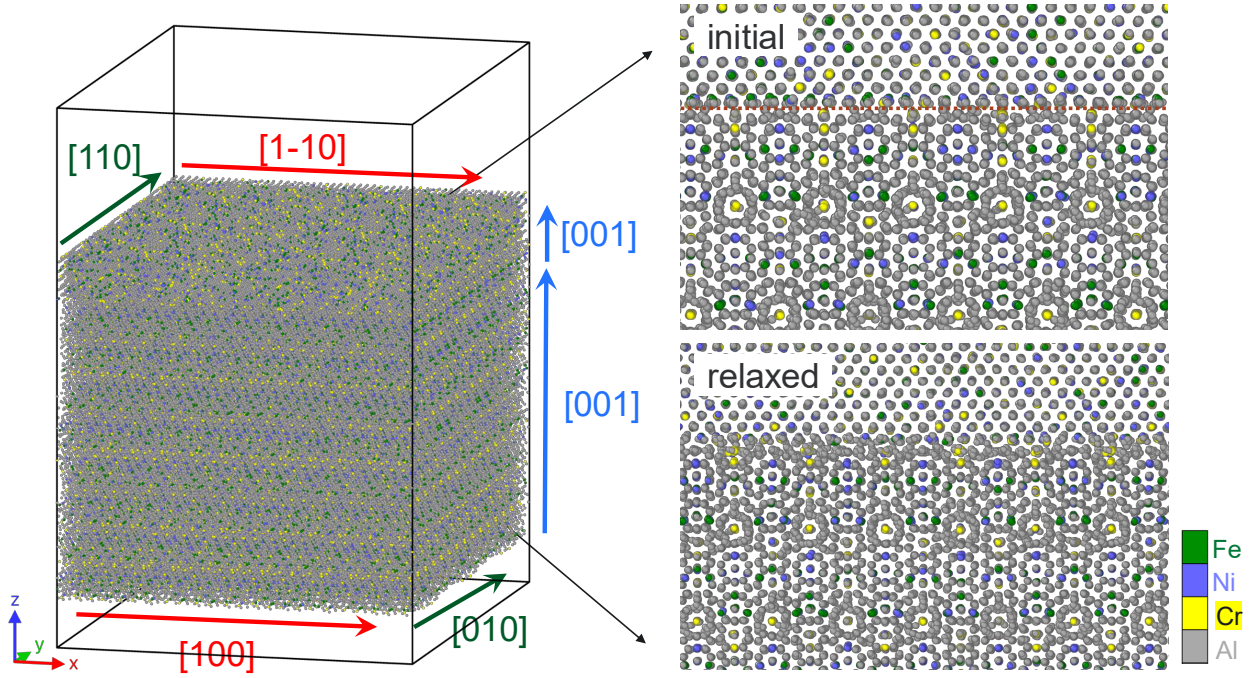

Figure 10. Crystal orientation, initial, and relaxed structures of QCA/fcc(001) interface.

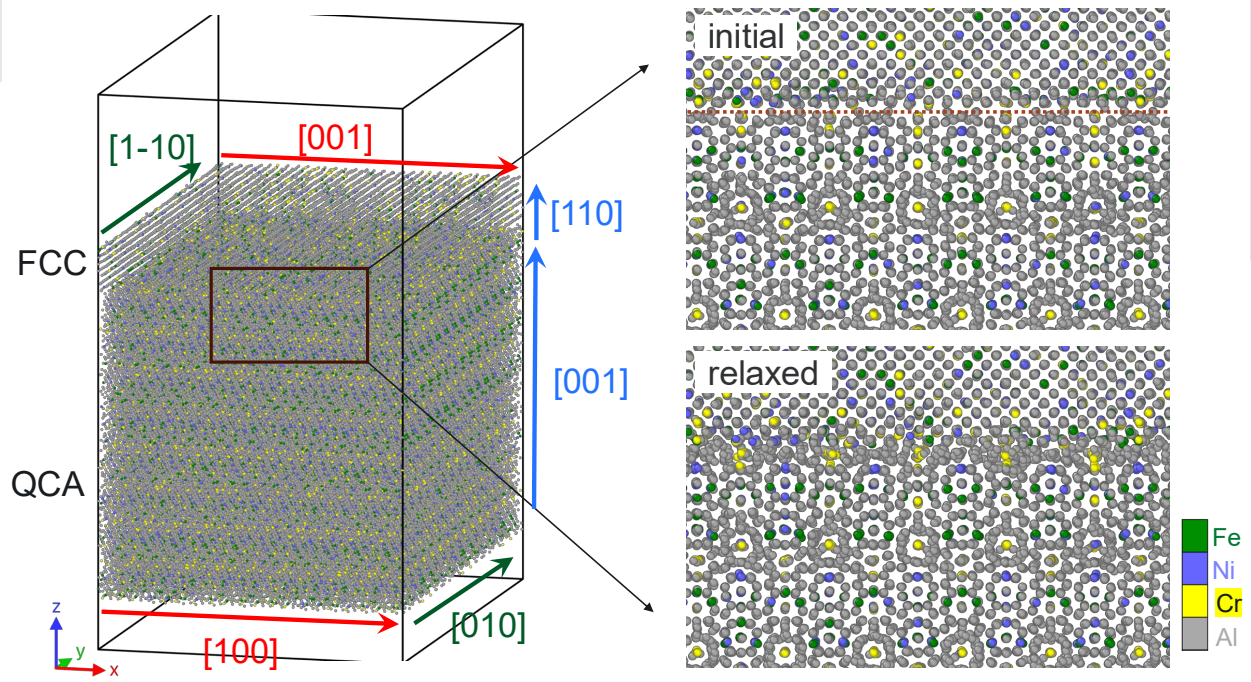

Figure 11. Crystal orientation, initial, and relaxed structures of QCA/fcc(110) interface.

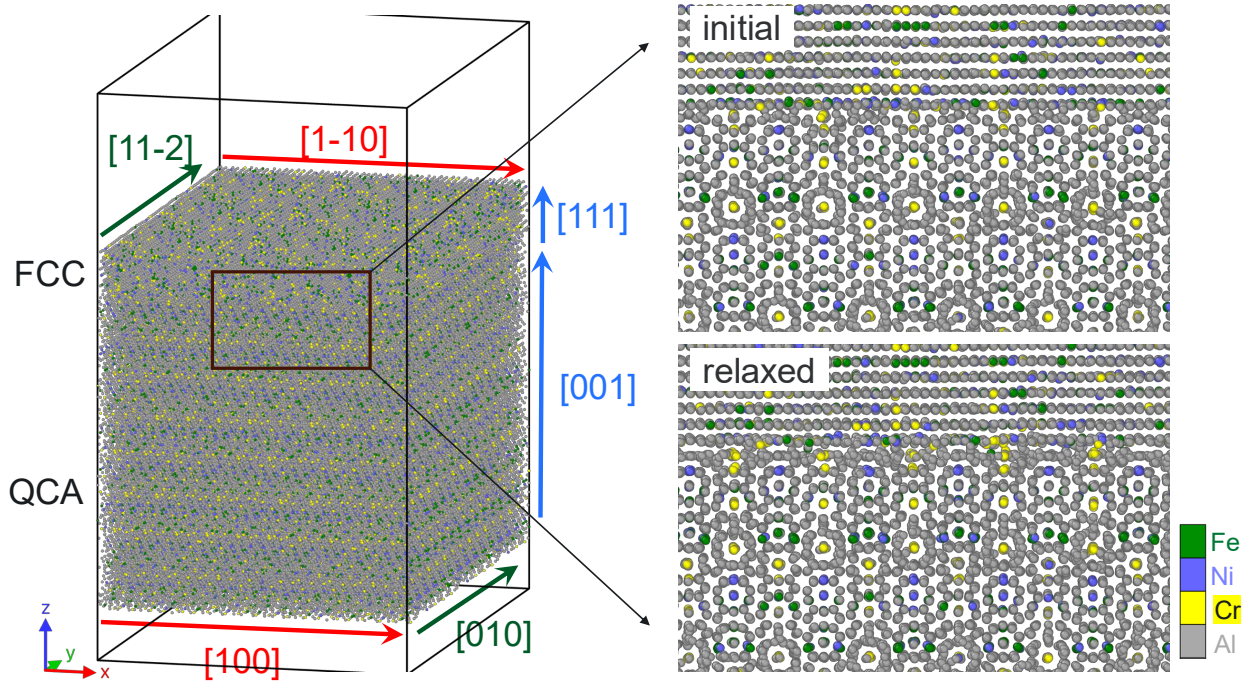

Figure 12. Crystal orientation, initial, and relaxed structures of QCA/fcc(111) interface.

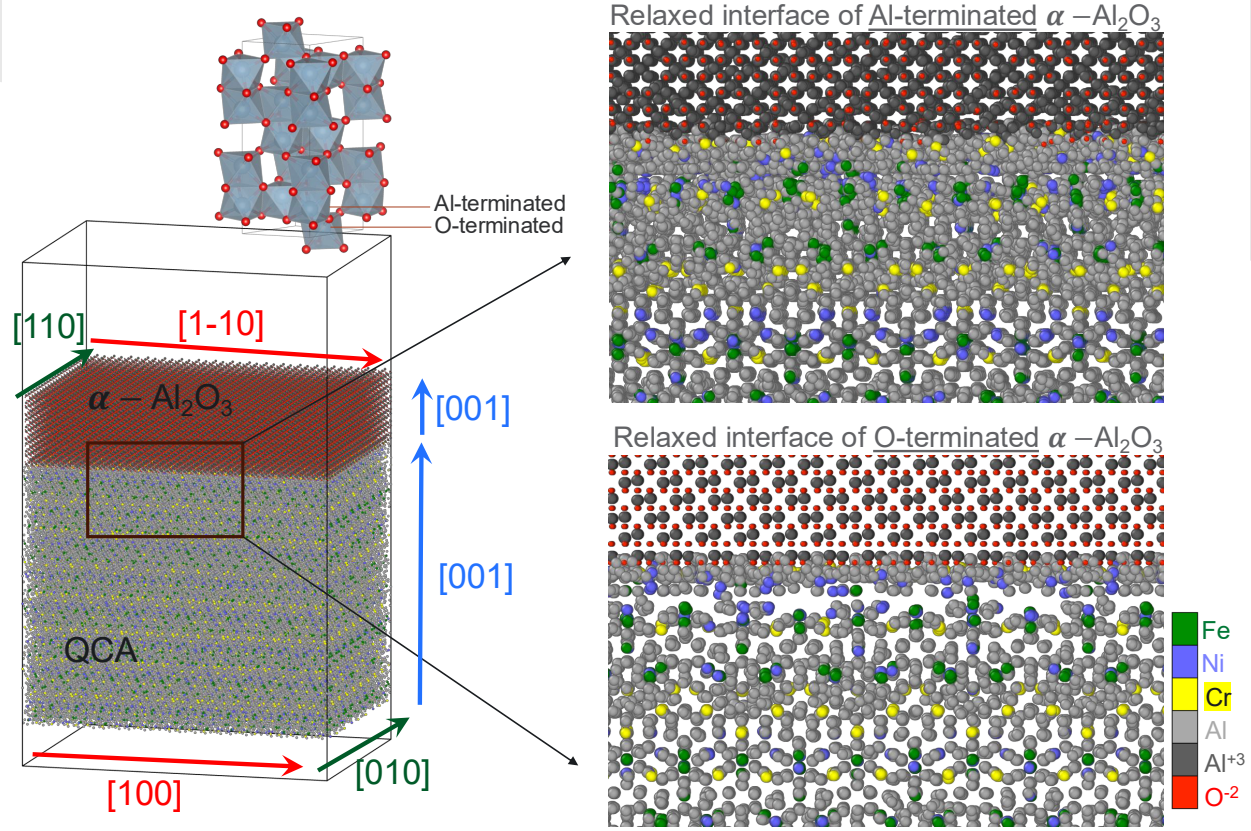

Figure 13. Crystal orientation, initial, and relaxed structures of QCA/α-Al_2O_3 interface.

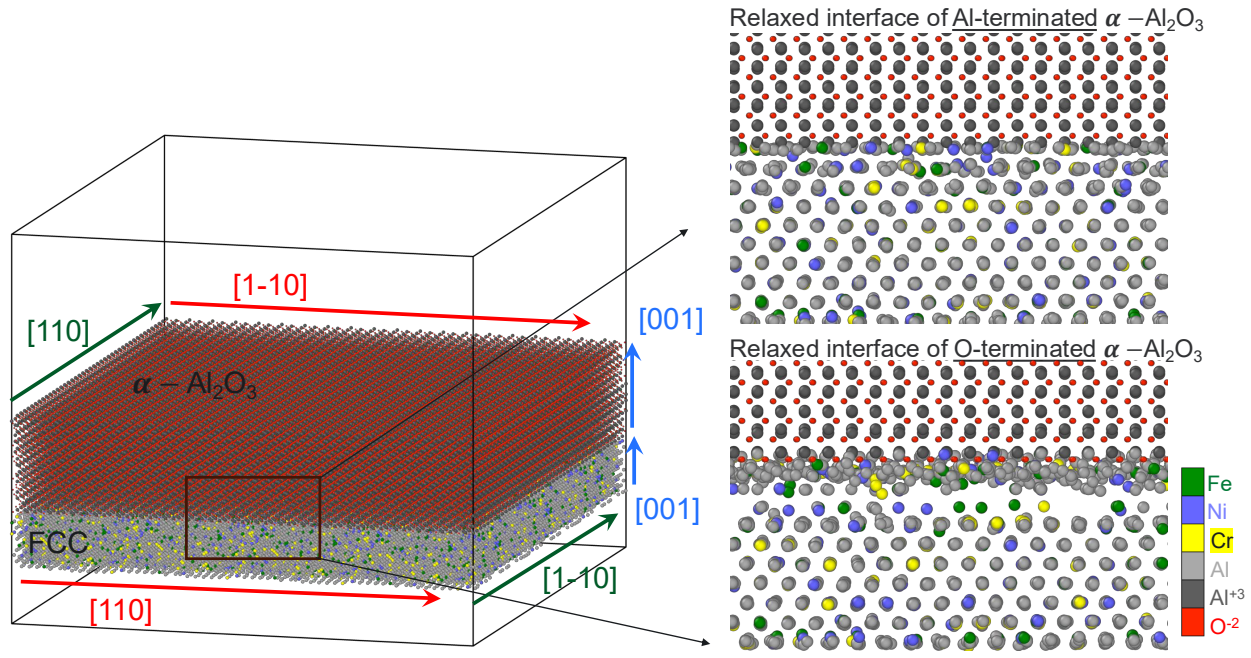

Figure 14. Crystal orientation, initial, and relaxed structures of α-Al_2O_3/fcc(001) interface.

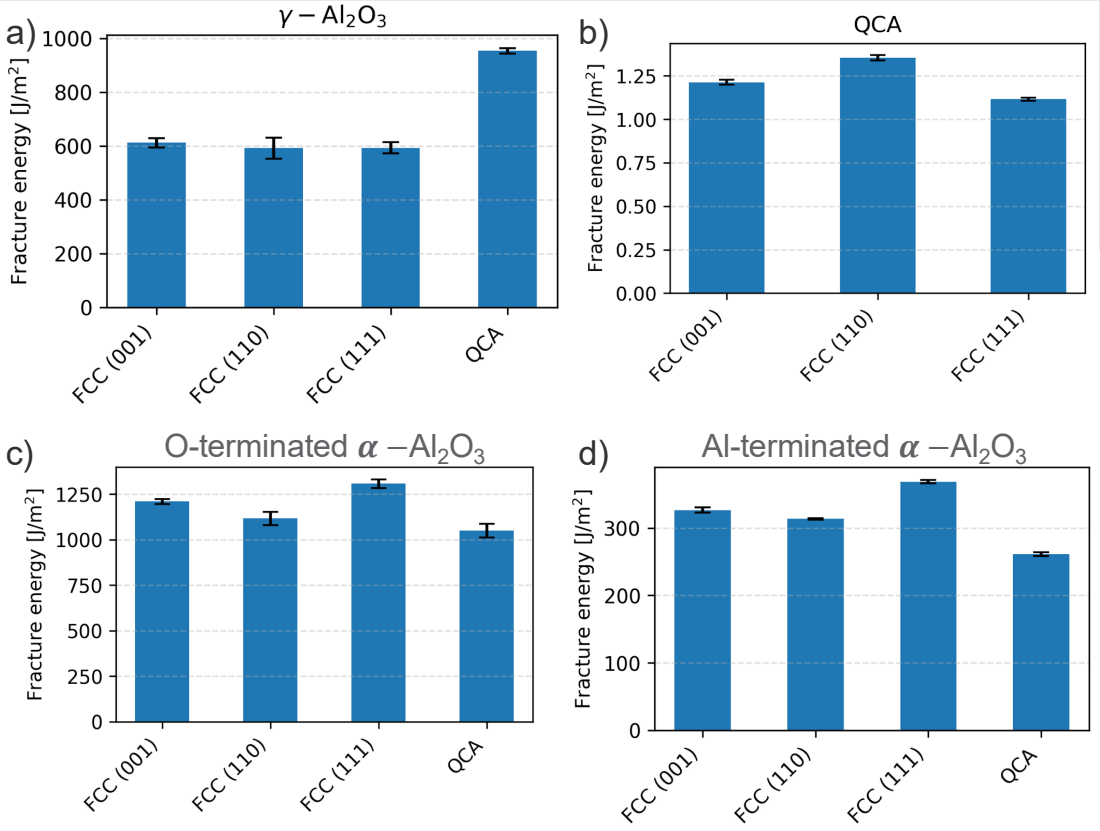

Figure 15. Fracture energies of interfaces obtained with the MEAM potentials + Buck/Coul potential tables. Error bars denote standard deviations.

3.2 Results with EAM Potentials

As previously mentioned, the MEAM potential which correctly predicts QCA to be more stable than fcc incorrectly predicts that an amorphous structure is more stable than fcc. At the composition studied here, the amorphous structure is more stable than fcc by 25.2 meV/atom. The tendency to form amorphous structure could affect the stability of the interlayer obtained with the MEAM potentials. Therefore, we test the EAM potentials for amorphization tendency. The calculations show that the EAM potentials correctly predict fcc to be more stable than amorphous by 31.8 meV/atom. Even though the EAM incorrectly predict the QCA to be less stable than fcc, to gain some insights into the effect of amorphization tendency on the interface structures, we also perform calculations using the EAM potentials + Buck/Coul potential tables. The interface structures are similar to those obtained with the MEAM potentials, thus not presented for brevity. The resulting fracture energies are shown in Figure 16. The results indicate that the fcc interlayer formation is not preferred between the QCA and γ-Al_2O_3, in agreement with the results with the MEAM potentials. However, unlike MEAM predictions that the interlayer is preferred between the QCA and α-Al_2O_3, the EAM potentials predict that it is only preferred for the Al-termination case. While for the O-terminated α-Al_2O_3, the interlayer formation remains not preferred.

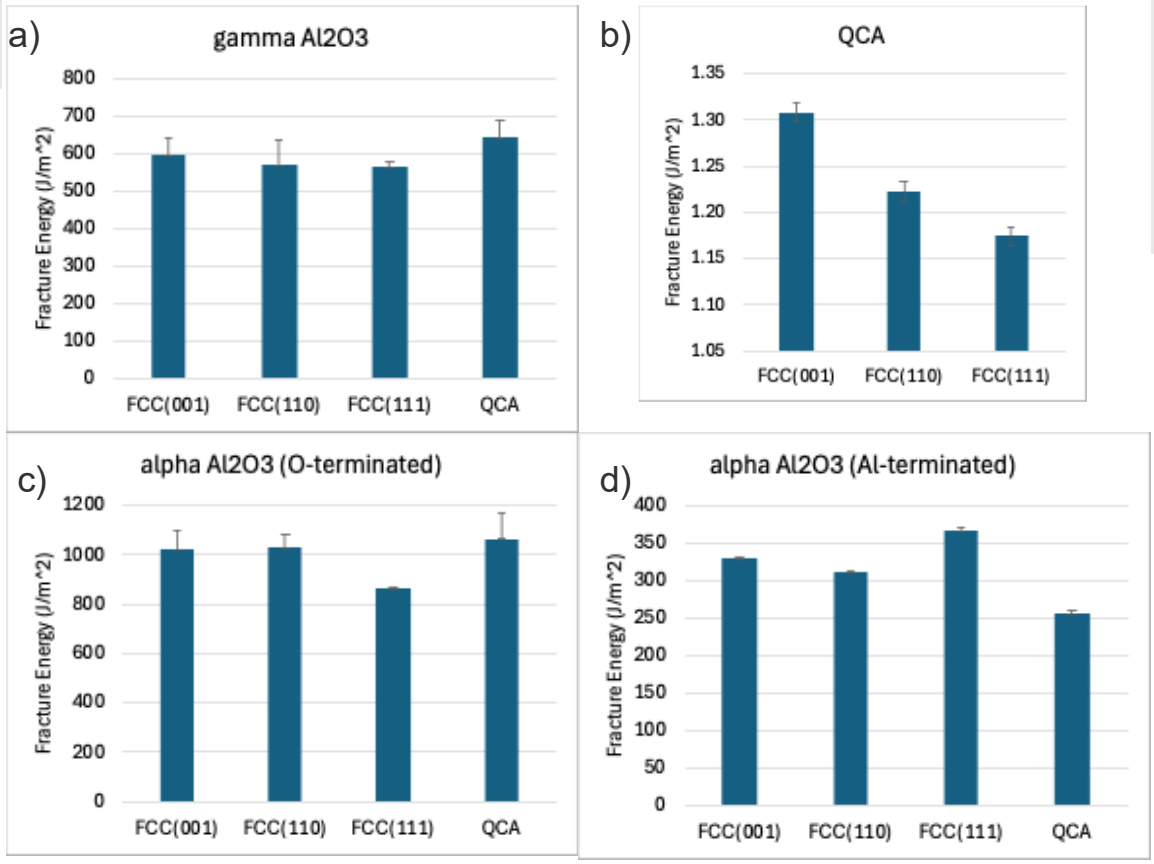

Figure 16. Fracture energies of interfaces obtained with the EAM potentials + Buck/Coul potential tables. Error bars denote standard deviations.

Conclusions

MEAM and EAM potentials have been used in conjunction with Buckingham/Coulomb interactions to explore the stability of an fcc interlayer between QCA and alumina interfaces. For the γ-Al_2O_3, both MEAM and EAM suggest that the fcc interlayer would not form. For the α-Al_2O_3, while the MEAM predicts that the fcc phase would form, the EAM gives a different prediction, where the fcc phase only forms for the Al-terminated α-Al_2O_3 at the interface. For the O-terminated α-Al_2O_3, the EAM predicts that the fcc phase would not form, consistent with the results for γ-Al_2O_3. In the current study, all simulations are performed in a closed system where atom exchange with an external reservoir is not considered. The discrepancy between MEAM and EAM for the α-Al_2O_3 suggests that the amount of oxygen may be important in influencing the interface structure. Future studies should consider oxygen exchange with an external reservoir to better model of the oxidation process. In addition, the interatomic potentials used in this study were developed independently for different systems. Therefore, there is a need to develop a consistent set of potentials fitted for the purpose of this study.

4.0 References

1. D. J. Edwards, D.J. Sunderland, A. Devaraj, A.L. Schemer-Kohrn, and B.E. Matthews. 09/23/2021. Post-irradiation Examination of Cycle 13 316SS Cladding Using Aberration-corrected STEM Imaging and Analysis, 6th Annual Tritium Science Technical Exchange, Richland, WA (2021), PNNL-SA-166684
2. Sui, H. X., X. Z. Liao, K. H. Kuo, and S. Hovmoller, Acta Crystallographica B53, 587 (1997)
3. Private communications with Matt Olszta
4. D. Farkas and A. Caro, Model interatomic potentials for Fe–Ni–Cr–Co–Al high-entropy alloys, Journal of Materials Research **35**, 3031 (2020)
5. H. Sharifi and C. D. Wick, Developing interatomic potentials for complex concentrated alloys of Cu, Ti, Ni, Cr, Co, Al, Fe, and Mn, Computational Materials Science **248**, 113595 (2025)
6. R. W. Grimes, *Solution of MgO, CaO, and TiO2 in α-AI2O3*. Journal of the American Ceramic Society **77**, 378-384 (1994)
7. R. W. Grimes, D. J. Binks, A. B. Lidiard, *The extent of zinc oxide solution in zinc chromate spinel*. Philosophical Magazine A **72**, 651-668 (1995)
8. L. Minervini, M. O. Zacate, R. W. Grimes, *Defect cluster formation in M2O3-doped CeO2*. Solid State Ionics **116**, 339-349 (1999)
9. L. Minervini, R. W. Grimes, J. A. Kilner, K. E. Sickafus, *Oxygen migration in LaNiO*. Journal of Materials Chemistry **10**, 2349-2354 (2000)